Ion-driven organic chemistry for Titan-like atmospheres: implications for N-dominated super-Earth exoplanets

Bourgalais, J.; Carrasco, N.; Miguel, Y.; Venot, O.; Pernot, P.

A&A 654, A171 (2021)
https://doi.org/10.1051/0004-6361/202141328

Astronomy & Astrophysics

Ion-driven organic chemistry for Titan-like atmospheres: Implications for N-dominated super-Earth exoplanets

J. Bourgalais[1,⋆], N. Carrasco[1], Y. Miguel[2], O. Venot[3], and P. Pernot[4]

[1] LATMOS, CNRS, UVSQ Université Paris-Saclay, Sorbonne Université; 11 boulevard d'Alembert, 78280 Guyancourt, France
e-mail: jeremy.bourgalais@univ-lorraine.fr
[2] Leiden Observatory, Leiden University, Niels Bohrweg 2, 2333 CA Leiden, The Netherlands
[3] Université de Paris and Univ Paris Est Creteil, CNRS, LISA, 75013 Paris, France
[4] Institut de Chimie Physique, CNRS, UPS Université Paris-Saclay, 310 rue Michel Magat, 91400 Orsay, France

Received 17 May 2021 / Accepted 28 July 2021

ABSTRACT

Context. Characterizing temperate (200–1000 K) super-Earth atmospheres is one of the future challenges in exoplanetary science. One of the major difficulties comes from the ubiquity of aerosols in these objects, which complicates the spectroscopic analyses. The knowledge gained on the Solar System is then crucial to better understand the chemical processes of exoplanet atmospheres.
Aims. This work focuses on the impact of ion chemistry on molecular diversity in a specific Titan-like exoplanet atmosphere that would be dominated by molecular nitrogen. On the largest satellite of Saturn, Titan, ion chemistry is a major component of molecular growth that forms precursors for the observed photochemical organic hazes.
Methods. Based on an experimental approach, we irradiated a gaseous mixture representative of a Titan-like atmosphere (N_2-dominated with CH_4) using an extreme-*uv* photon source (16.8 eV). Trace amounts of water vapor were added to the composition of the Titan-type gas mixture to simulate an exoplanet in the habitable zone.
Results. A wide variety of molecules and ions have been detected and they cannot all be identified based on our current knowledge of the organic chemistry of planetary atmospheres (mostly N- and C-based chemistry). The presence of even trace amounts of H_2O significantly broadens the product distribution, and H_3O^+ is found to be the most abundant ion.
Conclusions. This work demonstrates the complexity of the chemistry within exoplanet atmospheres. Numerical models must consider oxygen chemistry and ion-molecule reactions in order to probe the habitability of a certain type of super-Earths. The abundance of H_3O^+ makes it a good candidate for future observations.

Key words. planets and satellites: atmospheres

1. Introduction

Together with mini-Neptunes, super-Earths are part of a class of planets called Kepler planets, whose size is between that of the Earth and Neptune (1– 4 $R\oplus$, 1–30 $M\oplus$). Even if super-Earths do not exist in our Solar System (SS), they have the highest occurrence rate in the Milky Way, with almost a one-in-two chance of finding a super-Earth in orbit around a low-mass star (Mulders et al. 2018; Zhu & Wu 2018), the most common type of stars in the Galaxy (Dressing & Charbonneau 2013; Davenport et al. 2016). About 50% of the super-Earths would be located in the habitable zone (HZ) of their host star (Bonfils et al. 2013; Kopparapu et al. 2013), but they do not necessarily have the conditions to support liquid water oceans or Earth-like biology because their bulk composition can be very diverse according to their origin (Scora et al. 2020). The search for habitable super-Earths constitutes one of the main challenges in exoplanetary sciences and requires characterizing their atmospheres as well determining biosignatures (see, e.g., Schwieterman et al. 2018; Grenfell 2017; Seager et al. 2016 for recent reviews on the latter subject).

Transmission spectroscopy at visible or infrared wavelengths provides additional useful information about these relatively small planets, which are difficult to detect because they transit cold low-mass stars (Benneke & Seager 2012). Most of the planetary spectra obtained so far suggest that aerosols are ubiquitous in a number of exoplanet atmospheres (see, e.g., Ehrenreich et al. 2014; Knutson et al. 2014a), including super-Earths (Kreidberg et al. 2014; Knutson et al. 2014b). Aerosols constitute photochemical hazes and/or clouds that affect the thermal structure, dynamics, and more generally, the energy balance of atmospheres. The heating or cooling potential of the particles is determined by their abundance, composition, size, and shape, which define the optical properties (Zhang et al. 2017; Arney et al. 2016; Lavvas & Arfaux 2021). With their own broad spectral signatures, aerosols also obliterate the absorption features of gases and cause the planetary spectrum to be featureless. This hampers detecting the abundant heavy volatiles (Guo et al. 2020). The composition of the aerosols of cold rocky exoplanets and their major parent molecules thus remains largely unknown, although the chemistry of their atmosphere is known to be diverse (Hu et al. 2012; De Wit et al. 2018; Leconte et al. 2015; Owen & Mohanty 2016; Luger & Barnes 2015; Jin et al. 2014; Owen & Wu 2013).

It is then important to refer to the knowledge gained on the atmospheric chemistry of the SS planets. In this work, the focus is on exoplanets whose composition would be close to that of Titan, the main satellite of Saturn, which hosts a complex organic chemistry and photochemical hazes. Several super-Earth

⋆ Now at LRGP, CNRS, Université de Lorraine; 1 rue Grandville, 54001 Nancy, France.

simulations show that some of these worlds could have N-dominated atmospheres (De Wit et al. 2018; Angelo & Hu 2017; Hammond & Pierrehumbert 2017). An exoplanet in orbit around an M dwarf and receiving stellar irradiation equivalent to that of Titan will be located much closer to its host star and potentially in its HZ. The largest satellite of Saturn is thus a case that can be expected to be found outside the SS (Morley et al. 2015; Miguel 2019). The combination of the complex organic chemistry of Titan associated with the properties of planets in its HZ thus presents a sweet spot in prebiotic chemistry (Rahm et al. 2016; Hörst et al. 2012).

The atmosphere of Titan hosts aerosols, from the troposphere to the thermosphere (Tomasko et al. 2008; Vinatier et al. 2010; Koskinen et al. 2011), as well as many organic precursors, including ions that are major players in molecular diversity (Coates et al. 2007; Waite et al. 2005; Wahlund et al. 2009). The formation and growth of aerosols is directly linked to the ion chemistry, which form precursors through ion-molecule reactions (Waite et al. 2005; Cravens et al. 2006; Vuitton et al. 2007, 2009; Žabka et al. 2012; Lavvas et al. 2013). See MacKenzie et al. (2021) for a summary of the current state of knowledge on Titan.

The most recent models of hot and warm N-dominated super-Earth atmospheres include the formation of clouds and photochemical hazes with chemical equilibrium calculations (Mbarek & Kempton 2016; Mahapatra et al. 2017), or clouds that are based on the photodissociation of the most abundant gaseous chemical species (Zilinskas et al. 2020). The models consider the impact of the clouds on the thermal structure (Ito et al. 2015; Malik et al. 2019; Zilinskas et al. 2021) and atmospheric escape (Ito & Ikoma 2021). However, the size of molecular species remains limited (Arney et al. 2016; Kawashima & Ikoma 2018; Zahnle et al. 2016), and the impact of ion chemistry is currently not taken into account or at best is very limited (Morley et al. 2013; Kawashima & Ikoma 2018). Model development to simulate exoplanet atmospheres and aerosol formation is thus a real challenge because of the molecular diversity and elementary processes that must be taken into account to simulate all possible super-Earths.

The many chemical and physical parameters that are required for a good appreciation of the complex formation and evolution of aerosols can sometimes only be revealed by experimental studies. The few laboratory studies of exoplanets that have been performed so far of rocky planets have mainly focused on the composition of cloud or haze particles from various gas mixtures dominated by H_2, H_2O, and CO_2 (He et al. 2018a,c,b; Moran et al. 2020). The aim is to map all possible atmospheric compositions that could exist by exposing relevant gas mixtures in a vacuum chamber to an energy source (plasma discharge, *uv* lamp) that interacts with the molecules to form larger chemical species.

In a recent work, photochemical experiments using an extreme-UV photon source representative of M dwarf stellar radiation highlighted the main ions in an exoplanet atmosphere with a C/O ~ 1 ratio by irradiating a gaseous mixture of H_2–CO–N_2–H_2O (Bourgalais et al. 2020). Using the same experimental setup, this work focuses for the first time on the molecular diversity, in particular, of the ion that results from the irradiation of a Titan-based gas mixture of N_2–CH_4–H_2O with a mixing ratio of 0.95:0.05:0.003. This work is dedicated to the atmospheric chemistry of N-dominated exoplanets with C/O > 1 due to the presence of methane, an essential component for the photochemical haze formation (Kawashima & Ikoma 2018; Gao et al. 2020). The unavoidable presence of water vapor as the main trace species in the reactor (see further explanation in Sect. 2.1) allows us to study the impact of trace water vapor in this atmosphere of exoplanets. Water vapor is a key indicator of habitability and has already been detected in the atmosphere of mini-Neptunes (Tsiaras et al. 2019; Benneke et al. 2019). Its presence is one of the scenarios that is commonly considered for the analysis of the transmission spectra of super-Earths (De Wit et al. 2018). The greater abundance of CH_4 compared to H_2O allows for a reduced environment with an H/O > 10, which is known to favor molecular diversity and the development of prebiotic chemistry (Trainer 2013; Rimmer & Rugheimer 2019).

The paper is organized as follows. The first section briefly presents the experimental setup and the photochemical model we used to interpret the data. The second section presents an analysis of the neutral and ionized compounds that were detected. The identities of the species are given based on the numerical predictions of the photochemical model. A speculative identification of species that are not predicted is also made. The third and final section before the conclusion discusses lessons that can be learned for the molecular diversity of the atmosphere of Titan-like exoplanets and the impact on photochemical organic particles and cloud formation.

2. Experimental and numerical methods

2.1. UV irradiation of simplified exoplanetary atmosphere reproduced in the laboratory

A simplified N-dominated cold super-Earth atmosphere was reproduced in the laboratory using a stainless-steel ~5000 cm^{-3} parallelepipedal photochemical reactor that has been used in the past for photochemical experiments simulating complex environments similar to the upper layers of planetary (Carrasco et al. 2013; Peng et al. 2013; Bourgalais et al. 2019) and exoplanetary atmospheres (Bourgalais et al. 2020). The cell was filled using a flow regulator of 10 sccm (standard centimetric cube per minute) at room temperature and regulated by a vacuum system at a global pressure of ~100 Pa (1 mbar). We used a classical N_2/CH_4 (95/5%) gas mixture representing the atmosphere of Titan, provided by Air Liquide.

The inherent presence of water vapor in trace amounts due to micro-leaks of the reactor allowed us to consider a small source of oxygen in order to approach to some cases of super-Earths with H_2O in their atmosphere. Our reactor can be seen as an atmosphere that is constantly fed by the evaporation of a reservoir of liquid water (ocean or lake). The water signal was constant over time, and a relative abundance compared to N_2 of $\sim 3 \times 10^{-3}$ (see Fig. 1) was derived. A comparison between the intensity of the peaks normalized by their ionization cross section gives a reasonable estimate of the mole fraction. The good simulation of the ion chemistry using the photochemical model (see further explanation in Sect. 2.2) gives us confidence that there is no wall effect in the chemistry we probed and that the water mole fraction is correctly estimated.

The species of the gas mixture were then irradiated by a windowless EUV photon source coupled to the photochemical reactor produced by a microwave plasma discharge of a low-pressure inert neon flux providing radiation at 73.6 nm (NeI resonance line), corresponding to a photon energy of 16.8 eV, for a flux of about 10^{14} ph cm^{-2} s^{-1} (Tigrine et al. 2016; Bourgalais et al. 2019). The photoproducts present in the reactor were then sampled using a quadrupole m/z spectrometer (Hiden Analytical EQP 200 QMS) to measure neutral compounds and positive ions with high sensitivity below the parts per million (ppm) level (Bourgalais et al. 2019; Dubois et al. 2019, 2020). It is worth noting that the neutral molecules detected in this article are

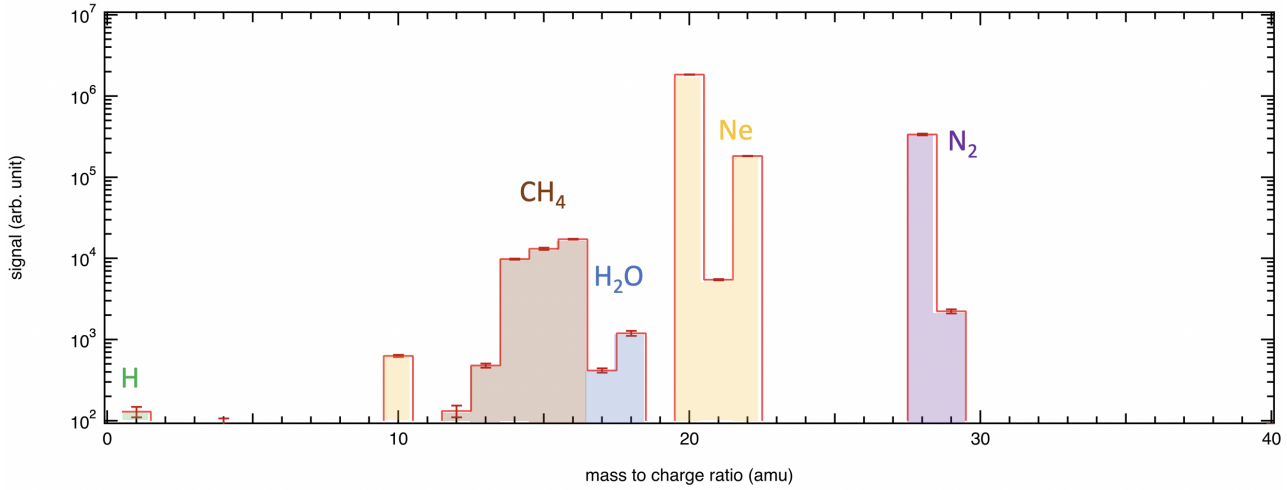

Fig. 1. In situ non-normalized gas-phase m/z spectrum of neutral species present in the reactor before EUV irradiation.

ionized fragments. In the following experimental m/z spectra, the uncertainties shown correspond to twice the standard deviation (2σ). The mass spectra reported in this study are the average of ten scans with an accumulation of 2 s amu^{-1} and channeltron-like detection over the 1–100 amu mass range. The chemical simulations (see Sects. 2.2 and 3.2.2) indicate that species reach their steady-state abundances in less than 1 ms. Acquisition of the mass spectra is started 5 min after the start of the irradiation, that is, largely after the system reaches its steady state.

The residence time of the molecules in the reactor and the 70 eV electron ionization of the spectrometer is very short, therefore it is difficult to identify the molecules that may form solely by observing the mass spectra of neutrals. In order to improve the detection of neutral molecules, the gas flow was passed through a cold trap maintained at the temperature of liquid nitrogen (77 K at atmospheric pressure) for 3 h, thus allowing the accumulation of condensable species (Gautier et al. 2011). At the end of each experiment, the cold trap still at the temperature of liquid nitrogen was exposed to a high vacuum (ca. 10^{-7} mbar) for 1 min to eliminate non-condensable species, before it was isolated, warmed to room temperature and opened on the photochemical reactor in static mode for m/z spectrometry measurement. This procedure is referred to as ex situ measurements in the rest of the paper as opposed to in situ measurements, which were done directly during the photoionization of the gas mixture. However, we cannot exclude that reactions can take place in the trap, and this should be kept in mind for the section on neutral species. The formation of ions is the main focus.

2.2. 0D photochemical model

To interpret the experimental m/z spectra, a photochemical 0D model was used to reproduce the chemistry obtained in the reactor. The photochemical model has already been described in the literature (Peng et al. 2014), and the main recent updates have been described in detail in its recent use for the interpretation of laboratory experiments that simulate the irradiation of exoplanet atmospheres (Bourgalais et al. 2020). Therefore, we only provide a summary here.

The model simulates chemistry under conditions similar to those of the experiments (Bourgalais et al. 2020). It is run for a time that is long enough to reach a steady state (0.1 s) and the stationary mole fractions of the products are compared with the experimental data. Complementary Monte Carlo simulations are performed to assess the uncertainty in the model predictions (500 runs). Subsequently, the confidence interval used in the results is 2σ, as in the experimental results. A global rate analysis is performed to identify the key reactions and dominant formation pathways.

The chemical model comprises 54 photoprocesses (photolysis of N_2, H_2, CH_4, C_2H_2, C_2H_4, C_2H_6, HCN, NH_3, CO, and H_2O), 903 neutral reactions (811 bimolecular and 92 termolecular), 1941 ion processes (1314 bimolecular and 687 dissociative recombinations), involving 177 neutral species, 190 positive ions of m/z up to 130, and electrons.

For a description of parameter uncertainty, see Peng et al. (2014). The database was initially focused on the chemistry of the elements H, C, and N and has recently been updated to include the oxygen species of Vuitton et al. (2019) and of the KIDA database (Wakelam et al. 2012).

3. Results

Figure 1 shows a gas phase in situ m/z spectrum of neutral species in the reactor before EUV irradiation of an N_2–CH_4–H_2O gas mixture at 1 mbar pressure. The species are detected at m/z 1, 10, 11, 12, 13, 14, 15, 16, 17, 18, 20, 21, 22, 28, 29, and 32. m/z 1, 12, 13, 14, and 15 correspond to the formation of H, C, CH, CH_2, and CH_3, which are the methane fragments (CH_4) at m/z 16. m/z 17 and 18 are attributed to OH and H_2O, respectively. Because of the high sensitivity of the m/z spectrometer, H_2O is detected as the source of oxygen in the reactor, and OH comes from the fragmentation of H_2O in the m/z spectrometer. m/z 10, 20, 21, and 22 are attributed to the twice ionized neon, Ne, and its isotopes (^{21}Ne, ^{22}Ne), respectively. Neon is used to produce EUV photons, but does not interact with the chemistry in the reactor (Tigrine et al. 2016). M/z 28 and 29 are attributed to molecular nitrogen N_2 and its first isotope $^{14}N^{15}N$.

3.1. Neutral species

Figure 2 shows ex situ spectra obtained for neutral species with and without irradiation in the photochemical chamber. The difference to Fig. 1 is that the gas in the reactor was flowing through a cryogenic trap, and thus condensable species were trapped during 3 h to improve the detection of photochemical products. The difference between the two spectra in Fig. 2 is based on the activation of the VUV source, to measure the contamination level of the reactor. In the ex situ spectrum resulting from condensation without photochemistry (blue spectrum in

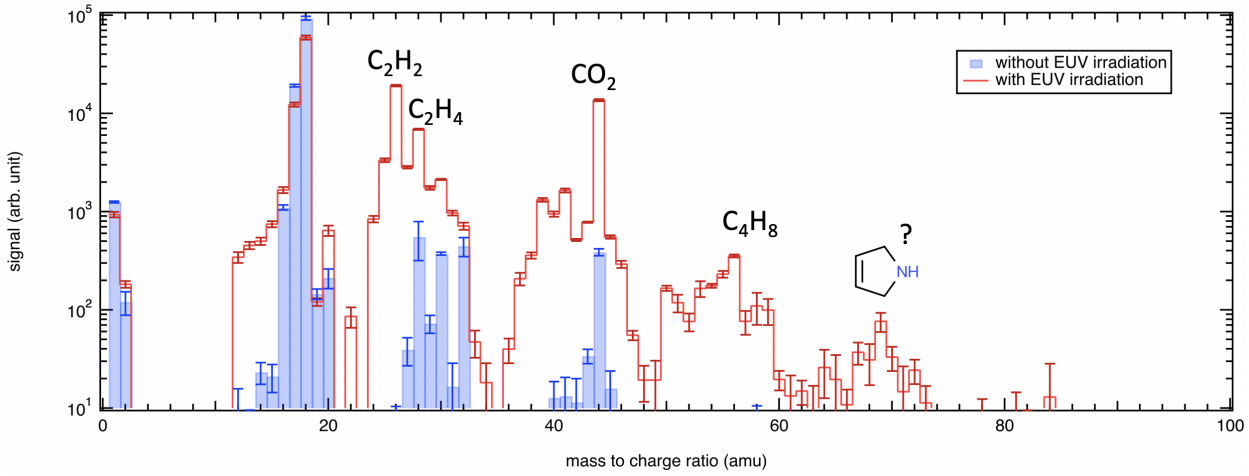

Fig. 2. Ex situ experimental m/z spectra obtained for neutral species with a N_2–CH_4–H_2O gas mixture with (red) and without (blue) irradiation in the photochemical chamber by using a 3-hour cryogenic trapping system.

Fig. 2), the main signatures that could be observed at m/z 28, 30, 32, 40, and 44 are attributed to CO, formaldehyde, O_2, Ar, and CO_2 (resulting from residual air from micro-leaks). It is worth noting that with a much better sensitivity, these trace species could have been directly observed in situ.

The ex situ spectrum resulting from condensation with photochemistry (red spectrum in Fig. 2) shows the impact of molecular growth by EUV photons. Without irradiation, the number, size, and intensity of the molecules are much smaller than when the molecules are irradiated, where several m/z of up to 100 amu are observed. The most notable peaks are those of water, acetylene (C_2H_2), ethylene (C_2H_4), and carbon dioxide (CO_2) at m/z 18, 26, 28, and 44, respectively. C_2H_2 and C_2H_4 are the first two hydrocarbons to form in a photochemical system dominated by N_2, CH_4 and water. Photolysis of CH_4 in EUV leads to a significant branching fraction of methyl ions CH_3^+, about 50%, which by reaction with CH_4 leads to the formation of ethyl ions ($C_2H_5^+$). These ions are then highly reactive with H_2O and lead to the formation of hydronium ions (H_3O^+) by reaction transfer as well as C_2H_4. Subsequently, successive photolysis of C_2H_4 leads to the formation of C_2H_2 directly through the successive loss of two H atoms, but mainly indirectly through the formation of $C_2H_3^+$ and $C_2H_4^+$ ions. As part of their main loss pathways, electronic recombination leads to the formation of C_2H_2,

$$CH_4 + h\nu(73.6\,nm) \longrightarrow CH_3^+ + H + e^- \quad (R1)$$
$$CH_3^+ + CH_4 \longrightarrow C_2H_5^+ + H_2 \quad (R2)$$
$$C_2H_5^+ + H_2O \longrightarrow H_3O^+ + C_2H_4. \quad (R3)$$

H_3O^+ is also at the origin of the formation of CO_2 through its recombination with electrons to form oxygen atoms, which will give CO_2 by reaction with the formyl radical (HCO). HCO is formed through the electronic recombination of CH_2OH^+, which is an abundant ion coming from the reaction between CH_2^+ + H_2O (see m/z 31 in Fig. 3),

$$H_3O^+ + e^- \longrightarrow O(^3P) + H_2 + H \quad (R4)$$
$$O(^3P) + HCO \longrightarrow CO_2 + H. \quad (R5)$$

In the fourth and fifth blocks observed in the irradiated spectrum of Fig. 2, m/z 56 and 69 stand out clearly. M/z 56 corresponds to the formation of butene isomers (C_4H_8) that form easily through the second exit pathway of methane photolysis at this wavelength, which forms the methane ion (CH_4^+). The

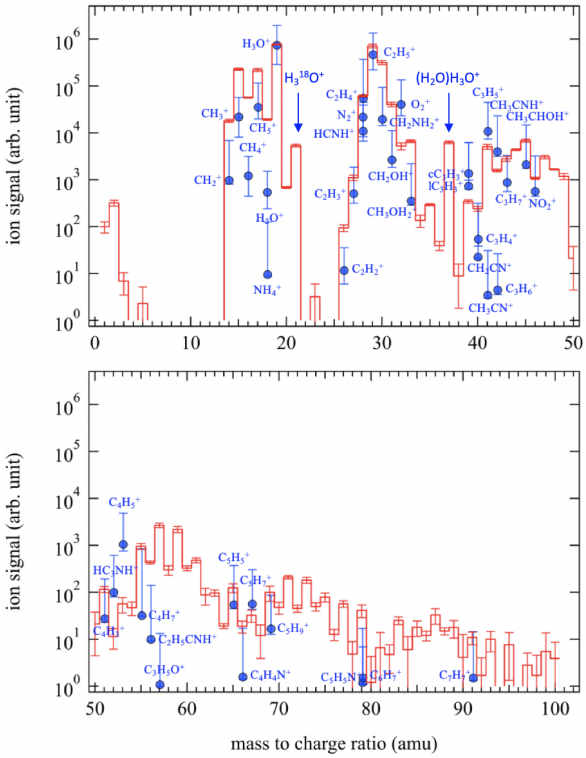

Fig. 3. *Upper panel*: m/z spectrum up to m/z 50. The names of the main ions as predicted by the photochemical model, and their relative abundance is symbolized by the blue dots. *Lower panel*: m/z spectrum from m/z 50 to m/z 100. The names of the main ions as predicted by the photochemical model, and their relative abundance is symbolized by the blue dots. Experimental and numerical data are scaled to m/z 29. The uncertainties on both experimental and numerical predictions are given as boxplots at a 2σ confidence interval.

reaction of this ion with CH_4 results in a proton transfer for the formation of the methanium ion (CH_5^+) and the methyl radical (CH_3). The latter is known to form C_4H_8 through its association reaction with the allyl radical (C_3H_5), for which the shortest production pathway comes from the reaction CH_2 + C_2H_4,

$$CH_4 + h\nu(73.6\,nm) \longrightarrow CH_4^+ + e^- \quad (R6)$$
$$CH_4^+ + CH_4 \longrightarrow CH_5^+ + CH_3 \quad (R7)$$
$$CH_3 + C_3H_5 \longrightarrow C_4H_8. \quad (R8)$$

The formation of unsaturated hydrocarbons such as the C_4H_8 isomers is very important because their high reactivity with radicals is responsible for efficient molecular growth in planetary atmospheres. These reactions have no activation barrier and several exit channels, thus promoting the molecular complexity through addition-elimination processes. In this case, *m/z* 56 correlates with *m/z* 69, which dominates the fifth block. At this m/z, no hydrocarbons are formed, but the insertion of a nitrogen atom in the raw formula leads to C_4H_7N isomers. More specifically, nitrogen atoms in their excited state, $N(^2D)$, resulting from the photolysis of N_2 with a branching ratio of 21%, may react with isomers of C_4H_8, leading to the formation of the cyclic amine 3-pyrroline (C_4H_6NH),

$$N_2 + h\nu(73.6\,nm) \longrightarrow N(^4S) + N(^2D) \quad (R9)$$

$$N(^2D) + C_4H_8 \longrightarrow C_4H_6NH + H. \quad (R10)$$

Other isomers such as butyronitrile (C_3H_7CN) can be considered, but its formation requires a nitrogen intermediate resulting from a succession of reactions, making C_4H_6NH the most probable compound at *m/z* 69,

$$C_2H_4CN + CH_3 \longrightarrow C_3H_7CN. \quad (R11)$$

Signals are also present at even larger m/z at the end of the spectrum, but the signal-to-noise ratio does not allow us to be affirmative. However, there are uncertainties that allow a signal to be validated at certain m/z (see *m/z* 78, 81, and 82), suggesting the formation of cyclic or linear nitrogen compounds or hydrocarbons, such as benzene. Compounds containing oxygen atoms may also be present, but this chemistry is less well known than that of carbon and nitrogen.

Further identification of the signals observed in the m/z spectrum of Fig. 2 remains difficult because the number of possible molecules increases with higher m/z. In addition, detection by m/z spectrometry leads to significant fragmentation of species and the trapping of molecules depends on their ability to condense. As mentioned in the description of the experimental protocol, spurious reactions in the trap can also alter the mass spectra of molecules. These aspects are a reminder that analysis of these molecule data is difficult and may be biased.

The remainder of this article is therefore focused on the analysis of positive ion measurements in situ. Their detection is facilitated by their positive charge, which allows us to guide them to the detection system without interferences. In addition, as mentioned earlier in this subsection, at this wavelength, photolysis of the primary compounds in the gas mixture predominantly results in the formation of ions that, through ion-molecule reactions initiate the molecular growth of the system. The ions are thus an indirect but unbiased indicator of the neutral molecules that are also formed in the reactor.

3.2. Ions

3.2.1. Experimental mass spectrum

During irradiation of the gas mixture in the reactor by the EUV photon source, many positive ions were detected (see Fig. 3). Signals up to m/z 100 is similar to what was observed in the m/z spectrum of neutral molecules, but results from 3 h of accumulation in a cryogenic trap. This result demonstrates the ubiquity of ions and their key role in molecular growth. Major ions reach their stationary state in times of about a tenth of a microsecond, while the first-formed neutral C_2H_4, if we exclude H and H_2, reaches its stationary state in a time of about some ms. In addition, ion mole fractions are not negligible compared to the neutrals because the most abundant ions are of about some ppm and the most abundant neutrals of about some ten ppm based on numerical predictions. This underlines the importance of ion-molecule chemistry on molecular growth, which is almost instantaneous compared to neutrals.

3.2.2. Comparison with numerical predictions

In order to identify the species formed at each m/z, a 0D photochemical model was used to reproduce the chemistry obtained from the gas phase contained in the reactor. Figure 3 shows the comparison of the simulated mole fractions of the ions predicted by the model with the measured experimental data. A relatively good agreement between experimental data and numerical predictions is observed in the first two blocks of the m/z spectrum. A shift begins within the third block, and this difference becomes more pronounced as the mass increases. Then a shift between predicted species and blocks is observed. The predicted species with the highest atomic m/z correspond to measured peaks but are not the most intense. In contrast, the predicted species correspond to weak signals that do not belong to the observed blocks. This demonstrates the presence of many molecules that are not predicted by models, even though they represent the most abundant complex species ($m/z > 50$) in the spectrum. Some heavy ions are present in the model, but act only as sinks of matter coming from lighter ions because we do not know their elementary reactions.

The upper panel of Fig. 3 reproduces the photochemical model well. It shows that the two most abundant ions in this environment are hydronium ions (H_3O^+) and small hydrocarbon ions. $C_2H_5^+$ is formed by reaction between CH_3^+ and CH_4, which comes from methane photolysis. H_3O^+ is subsequently formed through the reaction between $C_2H_5^+$ and H_2O, H_2O being the third most abundant molecule. The formation of H_3O^+ is also through a minor but efficient pathway that involves the reaction between CH_5^+ ions, from the reaction between CH_4^+ and CH_4, and H_2O,

$$CH_5^+ + H_2O \longrightarrow H_3O^+ + CH_4. \quad (R12)$$

The abundance of $C_2H_5^+$ and H_3O^+ supports the formation of the small neutral hydrocarbons observed at *m/z* 26 and 28 in the spectrum of Fig. 2. They are responsible for the molecular growth of neutral and charged species.

Hydrocarbons. The simulation of the mole fractions of hydrocarbons in the photochemical model shows the formation of large species containing up to six carbon atoms. The relative abundances of molecules such as $C_4H_3^+$, $C_4H_7^+$, $C_5H_9^+$, and $C_6H_7^+$ are in good agreement with the signals of m/z 51, 55, 69, and 79, respectively (see Fig. 3), as their growth mechanisms are known from studies of the planets of the SS and in particular, Titan (Vuitton et al. 2019). These hydrocarbons, which reach m/z approaching 80 atomic m/z units, are formed by ion-molecule reactions initiated by $C_2H_5^+$ and H_3O^+. Through electronic recombination and charge transfer reactions, it initiates m/z growth of both neutral and positively charged hydrocarbons. Thus with $C_2H_5^+$ and the small hydrocarbons C_2H_2 and C_2H_4, of which it is the origin, it is possible to describe the most efficient formation path for a heavy ion such as $C_6H_7^+$ (Westlake et al. 2014),

$$C_2H_5^+ + C_2H_2 \longrightarrow C_4H_5^+ + H_2 \quad (R13)$$

$$C_4H_5^+ + C_2H_4 \longrightarrow C_6H_7^+ + H_2. \quad (R14)$$

N-bearing species. The ions that formed include many nitrogenized compounds. Nitrogen species have lower relative abundances than hydrocarbons because unlike primary ions from methane photolysis, the main photoproduct from the N_2 photolysis, N_2^+, does not directly promote the formation of nitrogen ions, but acts as an additional source of small hydrocarbon ions (Imanaka & Smith 2007),

$$N_2^+ + CH_4 \longrightarrow CH_3^+ + H + N_2. \quad (R15)$$

Nitrogen atoms initiate the growth of nitrogen chemistry, but they represent only a minority of the products that are formed during the photolysis of molecular nitrogen at 73.6 nm. By reaction with small hydrocarbons, they initiate the insertion of a nitrogen atom in these molecules to form the first nitrogen species,

$$N(^4S) + CH_3 \longrightarrow H_2CN + H \quad (R16)$$
$$N(^2D) + CH_4 \longrightarrow CH_2NH + H. \quad (R17)$$

Then the ions H_3O^+ and $C_2H_5^+$ react with these small nitrogenized molecules to form the first nitrogenized ions by proton transfer,

$$H_3O^+/C_2H_5^+ + H_2CN \longrightarrow HCNH^+ + H_2O/C_2H_4 \quad (R18)$$
$$H_3O^+/C_2H_5^+ + CH_2NH \longrightarrow CH_2NH_2^+ + H_2O/C_2H_4. \quad (R19)$$

Then the growth of neutral and charged nitrogen molecules occurs sequentially by proton transfers and electronic recombinations until molecules with atomic m/z greater than 60 are formed, some of which have already been detected in planetary atmospheres, such as $C_2H_5CNH^+$ at m/z 56 (Vuitton et al. 2006),

$$N(^4S) + C_2H_3 \longrightarrow CH_2CN + H \quad (R20)$$
$$CH_2CN + CH_3 \longrightarrow C_2H_5CN \quad (R21)$$
$$H_3O^+ + C_2H_5CN \longrightarrow C_2H_5CNH^+ + H_2O. \quad (R22)$$

However, it should be noted that this growth of nitrogen molecules remains limited to molecules containing only one nitrogen atom because of the limit of fundamental knowledge in the literature. In contrast, the growth of hydrocarbons to the formation of large C-bearing molecules is so far much better understood than the growth of molecules containing nitrogen atoms.

Oxygenated species. H_3O^+ is the most abundant ion (cf. Fig. 2) and reacts by proton transfer or three-body association reactions to form heavier oxygen ions such as CH_2OH^+, $CH_3OH_2^+$, and CH_3CHOH^+, whose relative abundances correspond to the signals observed at m/z 31, 33, and 45, respectively (see R24 and R25),

$$H_3O^+ + C_xH_yO_z \longrightarrow C_xH_yO_zH^+ + H_2O \quad (R23)$$
$$H_3O^+ + C_xH_y + M \longrightarrow C_xH_yO_zH^+ + M. \quad (R24)$$

Additional pathways involving abundant hydrocarbon ions such as $C_2H_5^+$ also allow, by proton transfer with small oxygenated molecules, to contribute to the growth of the size of oxygenated ions (see R26),

$$XH^+ + C_xH_yO_Z \longrightarrow C_xH_yO_zH^+ + X. \quad (R25)$$

Protonated water clusters. Because H_3O^+ is the most abundant ion in the reactor, the formation of aggregate ions $H_3O^+(H_2O)$ is observed at m/z 37 although they are not predicted by the photochemical model (see R27),

$$H_3O^+(H_2O)_{n-1} + H_2O + M \longrightarrow H_3O^+(H_2O)_n + M. \quad (R26)$$

Water aggregates have higher proton affinities than water because H_3O^+ shares its charge with several molecules, which accentuates the stability (Hunter & Lias 1998). The greater the number of water molecules, the higher the proton affinity. For instance, the water dimer, $(H_2O)_2$, has a proton affinity of 808 kJ mol^{-1} compared to the 691 kJ mol^{-1} of H_2O (Goebbert & Wenthold 2004). It is also possible to detect the formation of aggregates larger than the dimer at m/z 55 and 73. Although at m/z 55, a hydrocarbon $C_4H_7^+$ is predicted, the large uncertainty related to its relative abundance cannot rule out the possibility that part of the signal at m/z 55 is related to the formation of the water trimer. As for m/z 71, its signal is the strongest in the block of which it is a part, suggesting that the formation of the water tetramer may also contribute to the observed signal.

3.2.3. Unidentified species

However, even though we used a model based on fundamental gas-phase knowledge of the chemical reactivity of carbon, nitrogen, and oxygen, many peaks above m/z 50 in the m/z spectrum in Fig. 3 remain unassigned. This discrepancy between model predictions and experimental observations becomes more pronounced as the atomic m/z units increase. The unidentified peaks each time correspond to a displacement of the blocks towards higher m/z, which may reasonably suggest that these unknown molecules contain oxygen atoms.

It is then reasonable to think that reactions such as proton transfer reactions with H_3O^+, which is very abundant, are missing from the photochemical model. As a source of proton transfer, H_3O^+ will react with most organic molecules because most organic molecules with proton affinity have values well below 900 kJ mol^{-1}. As an example, by reaction with acetone (CH_3COCH_3), proton transfer with H_3O^+ can lead to the formation of protonated acetone ($CH_3COCH_4^+$) to explain the relatively abundant signal observed at m/z 59 in block 4 of the m/z spectrum of Fig. 3 (Mackay et al. 1979; Bohme et al. 1979),

$$H_3O^+ + e^- \longrightarrow O(^3P) + H_2 + H \quad (R27)$$
$$O(^3P) + C_2H_4 \longrightarrow CH_3CO + H \quad (R28)$$
$$CH_3CO + CH_3 \longrightarrow CH_3COCH_3 \quad (R29)$$
$$H_3O^+ + CH_3COCH_3 \longrightarrow CH_3COCH_4^+ + H_2O. \quad (R30)$$

Proton transfer reactions with H_3O^+ are not favored with alkanes because their reactions are endothermic. However, the larger the size of the molecules, the more the proton transfer reactions with H_3O^+ become exothermic (Arnold et al. 1998). Reactions with hexane (C_6H_{14}) can thus be at the origin of the m/z 87, which dominates between m/z 80 and 90 in the spectrum of Fig. 3. However, it is also possible to see association reactions in competition with proton transfers (Španěl & Smith 1998a),

$$H_3O^+ + C_nH_{2n+2} + M \longrightarrow H_3O^+C_nH_{2n+2} + M. \quad (R31)$$

Other reactions that are not taken into account in the photochemical model may also occur. For H_3O^+, there are dehydration reactions especially in the case of heavy alcohols with at least

three carbon atoms but also carbonyl molecules (C=O) such as heavy aldehydes (–CHO) and carboxylic acids (C(=O)OH) (see R33) (Spanel & Smith 1997; Španěl & Smith 1998b),

$$H_3O^+ + C_nH_{2n+1}OH \longrightarrow C_nH^+_{2n+1} + 2\,H_2O. \quad \text{(R32)}$$

The potential formation of protonated water clusters observed from the dimer peak to m/z 37 is another example showing that proton transfer reactions with H_3O^+ are not the only reactions to be considered. The proton affinity of the aggregates is higher than that of H_3O^+ and therefore some reactions will not take place with water aggregates or will be done by permutation of ligands (see R34) (Bohme et al. 1979; Midey et al. 2000),

$$H_3O^+(H_2O) + X \longrightarrow H_3O^+(X) + H_2O. \quad \text{(R33)}$$

In conclusion, the reactivity of H_3O^+ is not limited to proton transfers and many other reactions can occur under our experimental conditions of temperature and pressure. It should also be noted that no reaction in the model allows the integration of several heteroatoms (N, O) in a single molecule. However, recent laboratory experiments have shown that molecules containing two nitrogen atoms can be formed in a photochemical environment with a mixture of Titan-type gases N_2/CH_4 (Carrasco et al. 2021). Moreover, in this work, a progressive shift of the clumps to the right appears to show an incorporation of oxygen in the organic structures, and protonation can hardly explain this. Thus the knowledge about molecular growth remains limited to organic molecules comprising a nitrogen atom or an oxygen atom, even if the incorporation of several oxygen molecules can be easily achieved, for instance, through the O_2^+ ion, which is relatively abundant (cf. Fig. 3). By reaction with CH_4, it can lead to the formation of the ion $HCOOH_2^+$, which could explain the abundant signal at m/z 47 in the spectrum of Fig. 3 (Rowe et al. 1984).

4. Discussion

4.1. Molecular diversity of Titan-based atmospheres

An N_2–CH_4–H_2O gas mixture was irradiated with EUV photons at 73.6 nm. This mixture is dominated by nitrogen with traces of water vapor and aims to be representative of a Titan-based atmosphere in the HZ. In the photochemical reactor, numerous molecules as well as positive ions were detected up to atomic m/z units of 100, with mole fractions in the ppm range with respect to N_2 for the most abundant species. Molecular growth is mainly driven by efficient proton transfer reactions from the most abundant ions ($k > 10^{-9}$ cm^3 s^{-1}). Ion-molecule reactions are more efficient than barrier-free neutral reactions due to long-distance attractive forces. Association reactions including ions may also play a role in the chemistry of cold exoplanetary atmospheres. Three-body stabilized reactions predominate in the Titan atmosphere up to an altitude of ~750 km, which corresponds to a temperature of about 150–200 K (Anicich et al. 2003; Kobayashi et al. 2017). At the wavelength of 73.6 nm used in this work, the branching ratio of water photolysis mostly leads to the formation of H_2O^+ (>70%), but in planetary environments, the reaction of radicals such as OH can also significantly contribute to the molecular diversity.

We detected heavy ionized organic species such as $C_6H_7^+$, which are precursors of polycyclic aromatic hydrocarbons (PAHs). This result agrees with the significant abundance of organic species measured in the gas phase in previous mini-Neptune and super-Earth experiments (He et al. 2018c). PAHs contribute to the early chemistry and are potentially essential ingredients in biochemistry on habitable planets such as the primordial Earth (Allamandola 2011).

The detection of neutral and charged N-bearing species in this work highlights the potential for nitrogen chemistry in the N-dominated atmosphere of exoplanets to form precursors to prebiotic chemistry. N-heterocyclic are the building blocks of biological systems as subunits for the formation of deoxyribonucleic acid (DNA) and ribonucleic acid (RNA) while gaseous nitriles like HCN are a reservoir for the formation of the building blocks of life (Rimmer & Rugheimer 2019). The role of nitrogen in haze formation is also very important (Israël et al. 2005; Imanaka & Smith 2007, 2010; Trainer et al. 2012), but the pathways of nitrogen insertion into organic molecules is far from being fully understood. This result agrees with complex species that have been identified in laboratory experiments on super-Earths and mini-Neptunes, with a raw formula corresponding to various amino acids, nucleotide bases and sugar derivatives (Moran et al. 2020).

We also showed many O-bearing molecules due to water vapor traces. Species containing the elements of life (C, N, O) are precursors to the formation of amide bonds (–CO–NH–) characteristic of peptides and proteins. In most atmospheres, these elements are trapped in stable molecules such as N_2 or CO. However, in atmospheres irradiated by stars with a significant EUV flux, the energy is sufficient to break the strong molecular bonds. The small molecules that formed from the first reactions such as H_2CO and HCN are precursors for the formation of prebiotic molecules such as sugars (Cleaves II 2008). These precursors have already been identified in recent laboratory experiments on the formation of photochemical hazes in a simulated atmosphere of temperate and cold exoplanets (He et al. 2018c). Oxygenated molecules could also facilitate nitrogen fixation in organic molecules because the incorporation of oxygen in Titan experiments led to the observation of amino acids and nucleobases (Hörst et al. 2012; Sebree et al. 2018).

We also showed that H_3O^+ and $C_2H_5^+$ are the most dominant ions and that they contribute to the molecular growth through proton transfer. A previous study for exoplanet atmospheres dominated by hydrogen (C/O = 1) had also highlighted the importance of H_3O^+ (Bourgalais et al. 2020). We demonstrated that despite different chemical environments (oxidized versus reduced medium), H_2O reacts through efficient proton transfer reactions to form H_3O^+. The mixing ratio of water in the atmosphere need only be a few ppm to form H_3O^+ in relative abundance equivalent to the major molecules. However, the chemistry of H_3O^+ is clearly incomplete in the photochemical model because many products, especially at high m/z atomic units, remain unattributed (see another lack of data illustrated in Carrasco et al. 2008).

Significant amounts of H_3O^+ in the reactor also lead to the formation of the first protonated water clusters. These short-lived loosely bound supramolecules represent the initial stage in the condensation process and can reach significant concentrations in high-density regions of planetary atmospheres. Their broad absorption characteristics would allow us to evaluate the pressure in cloudless atmospheres, and these and such results should motivate us to continue laboratory and numerical research into the absorption of water clusters (Misra et al. 2014) .

4.2. Impact on photochemical haze and cloud formation

Proton transfer reactions are among the most important reactions in ionospheres because ions formed by stellar radiation as well

as prebiotic organic molecules can penetrate deep into planetary atmospheres. The abundance of chemical species is influenced by transport and chemical processes that play an important role in the production of macromolecules, which are precursors of aerosols. Ions have a higher particle-sticking coefficient than radicals, and charge effects lead to faster and more stable growth which will have a significant impact on coagulation, evaporation, and particle dynamics (Sekine et al. 2008). Ultimately, electrostatic interactions have an impact on the aerosol mass flux induced by the ionized fraction of the atmosphere. Charging effects would become increasingly important as particle size increases because large particles can accumulate charges and thus must be considered in numerical models (Simones & Loyalka 2015).

The identification of multiple O-rich molecules shows a complex process of molecular growth and photochemical organic particle formation that would take place in the atmosphere of Titan-type exoplanets. A reduced environment (C/O >1) would reduce the formation of organic particles (DeWitt et al. 2009; Sciamma-O'Brien et al. 2010), but the presence of O-bearing molecules may act as a trap for hydrogen and limit the formation of species with saturated low molecular weight, such as CH_4 and C_2H_6, which do not contribute to the formation of particles (Trainer et al. 2006). The inclusion of oxygen in photochemical organic particles also tends to increase the formation of aerosols (Hörst et al. 2018a,b; He et al. 2018a; Jovanović et al. 2020). Organic molecules with terminal O-functions such as aldehydes and carboxylic acids allow decreasing the vapor pressure for a higher condensation rate (Trainer et al. 2006).

The oxidation of aerosols also leads to a change in their direct spectroscopic properties. Gavilan et al. (2017, 2018) found that solid material produced from a Titan-like atmosphere with increased oxidation to mimic an early Earth-like exoplanet, has higher absorption in the UV and mid-IR due to multiple O-bearing functional groups (amide, hydroxyl, and carbonyl). Our results also support the need for specific refractive index measurements of clouds and hazes in atmospheric conditions representative of exoplanets. The refractive indices used in numerical models are currently based on hydrocarbon material and are far from representing the potential diversity of optical properties of exoplanet haze (Gao et al. 2020; Lavvas & Koskinen 2017).

Ultimately, particles that are cloud condensation nuclei have an impact on the formation of clouds and hazes and their radiative properties (Cahoy et al. 2010; Yu et al. 2020). Clouds and hazes can promote habitability by impacting planetary albedo, atmospheric temperature structure, and chemical composition down to the surface (Helling 2019; Arney et al. 2017). They would allow habitable planets even with stellar fluxes more energetic than those received on Earth (Kopparapu et al. 2017; Bin et al. 2018; Arney et al. 2017). Planets orbiting M-type stars with slow rotation periods may have more water-rich stratospheres (mixingratio $> 10^{-3}$) that the Earth (around 1 ppm) (Benneke et al. 2019). When an exoplanet has an equilibrium temperature close to that of the Earth, water vapor can thus condense in the atmosphere. This is supported qualitatively in this work by the presence of the protonated water dimer, and it suggests that large molecular structures, so-called clusters, can begin to form and grow to condensation nuclei in relatively water-rich atmospheres. This is consistent with models that consider the formation of aggregate particles (Arney et al. 2016; Adams et al. 2019; Ohno et al. 2020).

5. Conclusion

The atmospheres of super-Earths cover a wide range of chemical compositions as well as temperature and pressure conditions. Thus, they can harbor a wide variety of molecules and ions. The growth of molecular diversity ultimately leads to the formation of clouds and hazes, but knowledge of the composition of their particles is critical in order to assess their impact on the radiative balance, climate and observability of exoplanets.

This explorative study has revealed the molecular diversity that can form under conditions representative of the upper atmospheric layers of specific Titan-based exoplanets, including many oxygenated and N-bearing organic molecules of astrobiological interest. We also highlighted the impact that they may have ion chemistry in the atmosphere of N-dominated exoplanets driven by nonequilibrium processes. In addition to increasing the molecular diversity in the ionosphere, ions can directly influence the growth of photochemical organic particles. The growth of organic molecules is well understood up to species of sizes comprising two or even three carbon atoms; the role of water is little involved for light ions. However, water seems to have a predominant role for heavier ions, as we showed here, with a progressive shift toward high masses in the mass spectra, highlighting the presence of oxygen in organic molecules. Even in environments with trace amounts of water vapor, the formation of ions, especially those carrying O-atoms, must therefore be taken into account for the formation of prebiotic organic particles. Understanding the mechanisms by which gas-phase molecules form larger particles and possibly aerosols is of paramount importance to critically assess their role in the climate given the diversity of compositions of super-Earth atmospheres. Furthermore, due to the mole fraction we derived, H_3O^+ is a potential target for future space observations that would focus on the detection of ionized species within the atmospheres of exoplanets.

However, we also showed that it is not possible to identify all the species that can potentially form based on the literature knowledge on organic chemistry within SS planetary atmospheres. Laboratory experiments and theoretical calculations are thus required to ensure photochemical model development in order to simulate molecular growth in exoplanet atmospheres from gas-phase compounds to the formation of solid particles. These models must include accurate measurements of reaction rate coefficients and product branching ratios, which are sorely lacking. The laboratory simulation approach described in this article provides clear results that can directly be used by the exoplanet community and proposes avenues of study to prepare future space missions and the analysis of data from the observations that will be obtained.

Acknowledgements. N.C. and J.B. thank the European Research Council for funding via the ERC PrimChem project (grant agreement no. 636829). O.V. thanks the CNRS/INSU Programme National de Planétologie (PNP) and CNES for funding support.

References

Adams, D., Gao, P., de Pater, I., & Morley, C. V. 2019, ApJ, 874, 61
Allamandola, L. 2011, EAS Pub. Ser., 46, 305
Angelo, I., & Hu, R. 2017, ApJ, 154, 232
Anicich, V. G., Wilson, P., & McEwan, M. J. 2003, J. Am. Soc. Mass Spectrom., 14, 900
Arney, G., Domagal-Goldman, S. D., Meadows, V. S., et al. 2016, Astrobiology, 16, 873
Arney, G. N., Meadows, V. S., Domagal-Goldman, S. D., et al. 2017, ApJ, 836, 49
Arnold, S. T., Viggiano, A., & Morris, R. A. 1998, J. Phys. Chem. A, 102, 8881

Benneke, B., & Seager, S. 2012, ApJ, 753, 100
Benneke, B., Wong, I., Piaulet, C., et al. 2019, ApJ, 887, L14
Bin, J., Tian, F., & Liu, L. 2018, Earth Planet. Sci. Lett., 492, 121
Bohme, D., Mackay, G., & Tanner, S. D. 1979, J. Am. Chem. Soc., 101, 3724
Bonfils, X., Delfosse, X., Udry, S., et al. 2013, A&A, 549, A109
Bourgalais, J., Carrasco, N., Vettier, L., & Pernot, P. 2019, J. Geophys. Res.: Space Phys., 124, 9214
Bourgalais, J., Carrasco, N., Changeat, Q., et al. 2020, ApJ, 895, 77
Cahoy, K. L., Marley, M. S., & Fortney, J. J. 2010, ApJ, 724, 189
Carrasco, N., Alcaraz, C., Dutuit, O., et al. 2008, Planet. Space Sci., 56, 1644
Carrasco, N., Giuliani, A., Correia, J.-J., & Cernogora, G. 2013, J. Synchrotron Radiat., 20, 587
Carrasco, N., Bourgalais, J., Vettier, L., Genier, E., & Spezia, R. 2021, A&A, submitted
Cleaves II, H. J. 2008, Precamb. Res., 164, 111
Coates, A., Crary, F., Lewis, G., et al. 2007, Geophys. Res. Lett., 34
Cravens, T., Robertson, I., Waite, J. H., et al. 2006, Geophys. Res. Lett., 33
Davenport, J. R., Kipping, D. M., Sasselov, D., Matthews, J. M., & Cameron, C. 2016, ApJ, 829, L31
De Wit, J., Wakeford, H. R., Lewis, N. K., et al. 2018, Nat. Astron., 2, 214
DeWitt, H. L., Trainer, M. G., Pavlov, A. A., et al. 2009, Astrobiology, 9, 447
Dressing, C. D., & Charbonneau, D. 2013, ApJ, 767, 95
Dubois, D., Carrasco, N., Petrucciani, M., et al. 2019, Icarus, 317, 182
Dubois, D., Carrasco, N., Jovanovic, L., et al. 2020, Icarus, 338, 113437
Ehrenreich, D., Bonfils, X., Lovis, C., et al. 2014, A&A, 570, A89
Gao, P., Thorngren, D. P., Lee, G. K., et al. 2020, Nat. Astron., 1
Gautier, T., Carrasco, N., Buch, A., et al. 2011, Icarus, 213, 625
Gavilan, L., Broch, L., Carrasco, N., Fleury, B., & Vettier, L. 2017, ApJ, 848, L5
Gavilan, L., Carrasco, N., Hoffmann, S. V., Jones, N. C., & Mason, N. J. 2018, ApJ, 861, 110
Goebbert, D. J., & Wenthold, P. G. 2004, Eur. J. Mass Spectrom., 10, 837
Grenfell, J. L. 2017, Phys. Rep., 713, 1
Guo, X., Crossfield, I. J., Dragomir, D., et al. 2020, ApJ, 159, 239
Hammond, M., & Pierrehumbert, R. T. 2017, ApJ, 849, 152
He, C., Hörst, S. M., Lewis, N. K., et al. 2018a, ApJ, 156, 38
He, C., Hörst, S. M., Lewis, N. K., et al. 2018b, ApJ, 856, L3
He, C., Hörst, S. M., Lewis, N. K., et al. 2018c, ACS Earth Space Chem., 3, 39
Helling, C. 2019, Ann. Rev. Earth Planet. Sci., 47, 583
Hörst, S., Yelle, R., Buch, A., et al. 2012, Astrobiology, 12, 809
Hörst, S. M., He, C., Lewis, N. K., et al. 2018a, Nat. Astron., 2, 303
Hörst, S. M., He, C., Ugelow, M. S., et al. 2018b, ApJ, 858, 119
Hu, R., Seager, S., & Bains, W. 2012, ApJ, 761, 166
Hunter, E. P., & Lias, S. G. 1998, J. Phys. Chem. Ref. Data, 27, 413
Imanaka, H., & Smith, M. A. 2007, Geophys. Res. Lett., 34
Imanaka, H., & Smith, M. A. 2010, Proc. Natl. Acad. Sci. U.S.A., 107, 12423
Israël, G., Szopa, C., Raulin, F., et al. 2005, Nature, 438, 796
Ito, Y., & Ikoma, M. 2021, MNRAS, 502, 750
Ito, Y., Ikoma, M., Kawahara, H., et al. 2015, ApJ, 801, 144
Jin, S., Mordasini, C., Parmentier, V., et al. 2014, ApJ, 795, 65
Jovanović, L., Gautier, T., Vuitton, V., et al. 2020, Icarus, 113774
Kawashima, Y., & Ikoma, M. 2018, ApJ, 853, 7
Knutson, H. A., Benneke, B., Deming, D., & Homeier, D. 2014a, Nature, 505, 66
Knutson, H. A., Dragomir, D., Kreidberg, L., et al. 2014b, ApJ, 794, 155
Kobayashi, K., Geppert, W. D., Carrasco, N., et al. 2017, Astrobiology, 17, 786
Kopparapu, R. K., Ramirez, R., Kasting, J. F., et al. 2013, ApJ, 765, 131
Kopparapu, R. K., Wolf, E. T., Arney, G., et al. 2017, ApJ, 845, 5
Koskinen, T., Yelle, R., Snowden, D., et al. 2011, Icarus, 216, 507
Kreidberg, L., Bean, J. L., Désert, J.-M., et al. 2014, Nature, 505, 69
Lavvas, P., & Arfaux, A. 2021, MNRAS, 502, 5643
Lavvas, P., & Koskinen, T. 2017, ApJ, 847, 32
Lavvas, P., Yelle, R. V., Koskinen, T., et al. 2013, Proc. Natl. Acad. Sci. USA, 110, 2729
Leconte, J., Forget, F., & Lammer, H. 2015, Exp. Astron., 40, 449
Luger, R., & Barnes, R. 2015, Astrobiology, 15, 119
Mackay, G. I., Tanner, S. D., Hopkinson, A. C., & Bohme, D. K. 1979, Can. J. Chem., 57, 1518
MacKenzie, S. M., Birch, S. P., Horst, S., et al. 2021, PSJ, 2, 112
Mahapatra, G., Helling, C., & Miguel, Y. 2017, MNRAS, 472, 447
Malik, M., Kempton, E. M.-R., Koll, D. D., et al. 2019, ApJ, 886, 142
Mbarek, R., & Kempton, E. M.-R. 2016, ApJ, 827, 121
Midey, A. J., Arnold, S. T., & Viggiano, A. 2000, J. Phys. Chem. A, 104, 2706
Miguel, Y. 2019, MNRAS, 482, 2893
Misra, A., Meadows, V., Claire, M., & Crisp, D. 2014, Astrobiology, 14, 67
Moran, S. E., Hörst, S. M., Vuitton, V., et al. 2020, Planet. Sci. J., 1, 17
Morley, C. V., Fortney, J. J., Kempton, E. M.-R., et al. 2013, ApJ, 775, 33
Morley, C. V., Fortney, J. J., Marley, M. S., et al. 2015, ApJ, 815, 110
Mulders, G. D., Pascucci, I., Apai, D., & Ciesla, F. J. 2018, ApJ, 156, 24
Ohno, K., Okuzumi, S., & Tazaki, R. 2020, ApJ, 891, 131
Owen, J. E., & Mohanty, S. 2016, MNRAS, 459, 4088
Owen, J. E., & Wu, Y. 2013, ApJ, 775, 105
Peng, Z., Gautier, T., Carrasco, N., et al. 2013, J. Geophys. Res.: Planets, 118, 778
Peng, Z., Carrasco, N., & Pernot, P. 2014, GeoResJ, 1, 33
Rahm, M., Lunine, J. I., Usher, D. A., & Shalloway, D. 2016, Proc. Natl. Acad. Sci. U.S.A., 113, 8121
Rimmer, P. B., & Rugheimer, S. 2019, Icarus, 329, 124
Rowe, B., Dupeyrat, G., Marquette, J., et al. 1984, J. Chem. Phys., 80, 241
Schwieterman, E. W., Kiang, N. Y., Parenteau, M. N., et al. 2018, Astrobiology, 18, 663
Sciamma-O'Brien, E., Carrasco, N., Szopa, C., Buch, A., & Cernogora, G. 2010, Icarus, 209, 704
Scora, J., Valencia, D., Morbidelli, A., & Jacobson, S. 2020, MNRAS, 493, 4910
Seager, S., Bains, W., & Petkowski, J. 2016, Astrobiology, 16, 465
Sebree, J. A., Roach, M. C., Shipley, E. R., He, C., & Hörst, S. M. 2018, ApJ, 865, 133
Sekine, Y., Imanaka, H., Matsui, T., et al. 2008, Icarus, 194, 186
Simones, M. P., & Loyalka, S. K. 2015, Nucl. Technol., 189, 45
Spanel, P., & Smith, D. 1997, Int. J. Mass Spectrom. Ion Processes, 167, 375
Španěl, P., & Smith, D. 1998a, Int. J. Mass Spectrom., 181, 1
Španěl, P., & Smith, D. 1998b, Int. J. Mass Spectrom. Ion Processes, 172, 239
Tigrine, S., Carrasco, N., Vettier, L., & Cernogora, G. 2016, J. Phys. D: Appl. Phys., 49, 395202
Tomasko, M. G., Doose, L., Engel, S., et al. 2008, Planet. Space Sci., 56, 669
Trainer, M. G. 2013, Curr. Org. Chem., 17, 1710
Trainer, M. G., Pavlov, A. A., DeWitt, H. L., et al. 2006, Proc. Natl. Acad. Sci. U.S.A., 103, 18035
Trainer, M. G., Jimenez, J. L., Yung, Y. L., Toon, O. B., & Tolbert, M. A. 2012, Astrobiology, 12, 315
Tsiaras, A., Waldmann, I. P., Tinetti, G., Tennyson, J., & Yurchenko, S. N. 2019, Nat. Astron., 3, 1086
Vinatier, S., Bézard, B., de Kok, R., et al. 2010, Icarus, 210, 852
Vuitton, V., Yelle, R., & Anicich, V. 2006, ApJ, 647, L175
Vuitton, V., Yelle, R., & McEwan, M. 2007, Icarus, 191, 722
Vuitton, V., Lavvas, P., Yelle, R., et al. 2009, Planet. Space Sci., 57, 1558
Vuitton, V., Yelle, R., Klippenstein, S., Hörst, S., & Lavvas, P. 2019, Icarus, 324, 120
Wahlund, J.-E., Galand, M., Müller-Wodarg, I., et al. 2009, Planet. Space Sci., 57, 1857
Waite, J. H., Niemann, H., Yelle, R. V., et al. 2005, Science, 308, 982
Wakelam, V., Herbst, E., Loison, J.-C., et al. 2012, ApJS, 199, 21
Westlake, J., Waite, J., Carrasco, N., Richard, M., & Cravens, T. 2014, J. Geophys. Res.: Space Phys., 119, 5951
Yu, X., Hörst, S. M., He, C., et al. 2020, ApJ, 905, 88
Žabka, J., Romanzin, C., Alcaraz, C., & Polášek, M. 2012, Icarus, 219, 161
Zahnle, K., Marley, M. S., Morley, C. V., & Moses, J. I. 2016, ApJ, 824, 137
Zhang, X., Strobel, D. F., & Imanaka, H. 2017, Nature, 551, 352
Zhu, W., & Wu, Y. 2018, AJ, 156, 92
Zilinskas, M., Miguel, Y., Mollière, P., & Tsai, S.-M. 2020, MNRAS, 494, 1490
Zilinskas, M., Miguel, Y., Lyu, Y., & Bax, M. 2021, MNRAS, 500, 2197